AAPG BULLETIN

Salt-driven evolution of a gas hydrate reservoir in Green Canyon, Gulf of Mexico

Alexey Portnov, Ann E. Cook, Mahdi Heidari, Derek E. Sawyer, Manasij Santra, and Maria Nikolinakou

AAPG Bulletin published online 21 December 2018
doi: 10.1306/10151818125

Cite as: Portnov, A., A. E. Cook, M. Heidari, D. E. Sawyer, M. Santra, and M. Nikolinakou, Salt-driven evolution of a gas hydrate reservoir in Green Canyon, Gulf of Mexico, *(in press; preliminary version published online Ahead of Print* 21 December 2018*):* AAPG Bulletin, doi: 10.1306/10151818125.

Title:

Salt-driven evolution of a gas hydrate reservoir in Green Canyon, Gulf of Mexico

Authors:

Alexey Portnov[1,2*], Ann E. Cook[1], Mahdi Heidari[3], Derek E. Sawyer[1], Manasij Santra[3], Maria Nikolinakou[3]

[1] *School of Earth Sciences, The Ohio State University, Columbus, Ohio, USA*

[2] *CAGE - Centre for Arctic Gas Hydrate, Environment and Climate, Department of Geology, UiT The Arctic University of Norway, Tromsø, Norway*

[3] *Jackson School of Geosciences, The University of Texas at Austin, Austin, Texas, USA*

*Correspondence to:

Alexey Portnov

Email: portnov.1@osu.edu

Phone: +1 614 7952683

Present postal address for all authors:

125 Oval Dr S, Columbus, OH 43210, USA

1. Acknowledgments and Data

The authors would like to acknowledge Peter Flemings for his constructive comments on our paper and Adam Skarke for providing us with coordinates of hydroacoustic flares in Block GC955, Green Canyon protraction area, Gulf of Mexico. Author A. Cook acknowledges support from the NAS Gulf Research Program.

The industry log data and reports can be ordered from BOEM (Bureau of Ocean Energy Management) website: https://www.data.boem.gov. The 2D seismic data used in the current study can be obtained from NAMSS (The National Archive of Marine Seismic Surveys) website: https://walrus.wr.usgs.gov/namss/

Abstract

The base of the gas hydrate stability zone (GHSZ) is a critical interface, providing a first-order estimate of gas hydrate distribution. Sensitivity to thermobaric conditions makes its prediction challenging particularly in the regions with dynamic pressure-temperature regime. In Green Canyon in the northern Gulf of Mexico (Block GC955), the seismically inferred base of the GHSZ is 450 meters (1476 ft) below the seafloor, which is 400 m (1312 ft) shallower than predicted by gas hydrate stability modeling using standard temperature and pressure gradient assumptions, and an assumption of structure I (99.9% methane gas) gas hydrate. We use 3D seismic, log data and heat flow modeling to explain the role of the salt diapir on the observed thinning of the GHSZ. We also test the alternative hypothesis that the GHSZ base is actually consistent with the theoretical depth. The heat flow model indicates a salt-induced temperature anomaly, reaching 8 °C at the reservoir level, which is sufficient to explain the position of the base of the GHSZ. Our analyses show that overpressure does develop at GC955, but only within a ~500 m (1640 ft) thick sediment section above the salt top, which does not currently affect the pressure field in the GHSZ (~1000 m (328 ft) above salt). Our study confirms that a salt diapir

can produce a strong localized perturbation of the temperature and pressure regime and thus on the stability of gas hydrates. Based on our results, we propose a generalized evolution mechanism for similar reservoirs, driven by salt-controlled gas hydrate formation and dissociation elsewhere in the world.

2. Introduction

Gas hydrate is a solid, ice-like form of water and gas (mainly methane), which is stable at the specific envelope of temperature and pressure (Kvenvolden and Lorenson, 2001). Because of the particular stability regime, natural gas hydrates are found worldwide within the sediment on continental slopes, in the polar permafrost regions (Collett, 2002), and potentially even under the ice sheets (Portnov et al., 2016). In the ocean, the subbottom gas hydrate stability zone (GHSZ) thickness may exceed 1000 m (3280 ft), primarily controlled by pressure (water depth), geothermal gradient, gas composition, and pore water salt content (Kvenvolden and Lorenson, 2001). The base of GHSZ is a critical interface that determines the thickness of gas hydrate stability, below which gas hydrate is thermodynamically unstable (Haacke et al., 2007). Defining the base of the GHSZ is thus essential for estimation of gas hydrate volume, pore pressure prediction, safe borehole planning, and assessing submarine landslide potential (McIver, 1982; Frye, 2008; McConnell et al., 2012). The base of hydrate stability is often identified in seismic data from the geophysical signature – a bottom simulating reflection (BSR). In seismic data, a BSR is typically observed coincident with the base of GHSZ as a high-amplitude negative impedance contrast with reversed polarity from the water bottom reflector (Haacke et al., 2007). Heat flow and gas hydrate stability modeling are often used for characterization of GHSZ boundaries (Kvenvolden and Lorenson, 2001), and inversely, heat flow is interpreted based on the location of the BSR (Phrampus et al., 2017). While seismic surveys and theoretical hydrate phase boundary modeling have proved to be efficient in the areas with regionally uniform

geothermal heat flow, such as Blake Ridge on the southeastern U.S. passive margin (Wood and Ruppel, 2000), it may be more challenging on active margins, as shown for the Nankai Trough in the eastern Japan subduction zone (Kinoshita et al., 2011). Similarly, in the salt provinces like the Gulf of Mexico (Figure 1), salt tectonics may significantly distort both temperature and pressure fields and therefore change the configuration of the GHSZ (Ruppel et al., 2005; Frye, 2008).

Herein, we test the effects of salt diapirism on the stability regime of a gas hydrate reservoir in Green Canyon Block 955 (GC955) located in the northern Gulf of Mexico just off the edge of the Sigsbee Escarpment (~2000 m (6561 ft) water depth) (Figure 2a). Existing seismic and drilling data were previously used to estimate the base of the GHSZ at ~450 m (1476 ft) below the seafloor (mbsf) in GC955 (Boswell et al., 2012; Haines et al., 2017). This is 400 meters (1312 ft) shallower than the depth predicted by the theoretical gas hydrate phase boundary modeling (Sloan and Koh, 2008) for a regional, average geothermal gradient (20°C/km) (6°C/1000 ft) in the Green Canyon protraction area (Jones, 2003; Forrest et al., 2007). We explore several possible reasons for the mismatch in the estimated and modeled base of the GHSZ, which include: (1) assessing the potential effect of an underlying salt diapir on pore pressure and temperature gradient, and (2) testing the alternative hypothesis, that the actual base of the GHSZ depth is consistent with the theoretically predicted depth. Our modeling results support the salt diapir hypothesis due primarily to a high geothermal gradient as a primary reason for the shallow base of GHSZ.

This salt-diapir effect may be widespread where significant salt diapirism occurs across the Gulf of Mexico slope as well as in other offshore locations such as US East Coast, Brazilian and West Africa continental slopes, Mediterranean Sea, Persian Gulf (Figure 1); these regions usually

coincide with the temperature and pressure regime where gas hydrate is stable. Therefore, we propose a generalized evolution mechanism for salt diapir-roof gas hydrate reservoirs applicable to marine salt provinces worldwide.

3. Geologic setting and data sets

Upper sediment cover of the northern Gulf of Mexico fills a complicated synrift, mini-basin system created by the movement of Upper Jurassic allochthonous Louann salt deposits (Peel et al., 1995). In the Oligocene and Miocene, accumulation of thick Mesozoic and Cenozoic sediments mobilized this massive salt canopy and induced its upthrust towards the seafloor, forming sills, bulbs and diapiric domes of different size and shape (Jackson and Talbot, 1986; Peel et al., 1995). Associated salt tectonics is responsible for a large number of structural hydrocarbon traps, which constitute a significant part of the Gulf of Mexico's hydrocarbon reservoirs (Worrall and Snelson, 1989; Diegel et al., 1995).

For our seismic interpretation in GC955 we used a depth-migrated (zero-phase American SEG standard) seismic volume with the total record length of 14,000 m (8.7 ml), 30x25-m (98x82 ft) bin size and 8 ms sampling rate, provided by WesternGeco. A key feature imaged with these data is a prominent diapiric salt body with an apparent height of ~6 km, intruded into the Cenozoic sediment section (Peel et al., 1995) that ascends to within 1500 meters (4921 ft) of the seafloor (Figure 3a). Within the roof sediments above the diapir, a coarse-grained gas hydrate reservoir appears as a zone of anomalous high-amplitude reflections within a channel-levee system at 450-500 mbsf (1476-1640 ftbsf) (McConnell et al., 2010; Boswell et al., 2012; McConnell et al., 2012; Haines et al., 2017). The entire diapir roof section has a 4-way anticlinal structure related to the underlying salt diapir, and is intersected by normal faults rooted at the top of the salt diapir and many of which are restricted to the sand-rich facies (Santra et al., in press, this issue). High-

amplitude reflections occur near the crest of the anticlinal structure at the gas-hydrate bearing interval and below it (Figure 3a, 4a) (Haines et al., 2017). According to the existing logging-while-drilling (LWD) data, acquired under the Gulf of Mexico Gas Hydrate Joint Industry Project Leg II (Collett et al., 2012), the coarse-grained gas hydrate-bearing reservoir in vicinity of GC 955 H001 well is ~30 m (98 ft) thick. High compressional velocity (up to 3200 m/s) (10500 ft/s) and resistivity (10-100 ohm m) were measured in the gas hydrate-bearing reservoir, which suggests gas hydrate saturation up to 90% (Collett et al., 2012). Only one hole (GC 955 Q001) out of three drilled in the area during JIP Leg II indicated evidence of free gas underlying gas hydrate (Boswell et al., 2012). Gas hydrate structure 1 occurrence (99.9% methane gas) in the reservoir was confirmed in May, 2017, by drilling two twin holes GC 955 H002 and GC 955 H005 during expedition UT-GOM2-01 (Flemings et al., 2018). In the current study we use LWD data from two wells drilled into the roof of the salt diapir, JIP Leg II Hole GC 955 H001 (~570 mbsf TD (1870 ftbsf), true vertical depth) and industry well GC955 #001 (~2175 mbsf TD (7135 ftbsf), measured depth), in addition to one well drilled at the margin of the salt diapir, industry well GC955 #002 (~5843 mbsf TD [meters below sea floor, total depth)(19169 ftbsf), measured depth) (Figure 2a, b). We integrate well logs with 3D seismic data to constrain pore pressure and heat flow in GC955 study area.

The geothermal gradient in the Gulf of Mexico is not uniform. Geothermal gradients in industry wells from the Green Canyon protraction area are typically below 20 °C/km (6°C/1000 ft), however several wells show higher values (30-40 °C/km) (9.1-12.2 °C/1000 ft) (Jones, 2003; Forrest et al., 2007). These high geothermal gradients have been previously explained by the local heat-conductive salt effect (Mello et al., 1995; Frye, 2008). Wood et al. (2002) and Shedd

et al. (2012) also suggested that aerially-limited increases in heat flow due to intensive fluid flux in the Gulf of Mexico may generate "pluming BSRs", bowed toward the seafloor.

4. Methods

4.1 Pore pressure prediction from sonic and resistivity logs

Hydrostatic (P_h) and overburden (P_{ob}) pressure in the GC955 study area were calculated using the following equations (Zoback, 2007):

$$P_h = \rho_w g h;$$

$$P_{ob} = \rho_w g h_w + \rho_b g (h - h_w),$$

where ρ_w is water density g is acceleration due to gravity, h is total depth, h_w is water depth, and ρ_b is bulk density of the sediments from the density log. See Table 1 for values used.

For better accuracy and control, pore pressure calculations have been performed using two independent methods: from the compressional velocity log and from the selected resistivity log (Eaton's method) (Zoback, 2007). LWD data from Hole GC 955 H001 was acquired during the Gulf of Mexico gas hydrate Joint Industry Project, Leg II (Boswell et al., 2012); for pore pressure prediction using data from this hole, we use the compressional travel time and the RING resistivity measurement (the ring resistivity measured by a LWD toroid device). The data from Hole GC955 #001 were collected by Statoil Exploration Inc. in 1999 (McConnell, 2000), and we use the compressional travel time log and the PSR (phase shift resistivity) log. To characterize the pore pressure within the diapir roof sediments in GC955, we combined LWD log data from GC 955 H001 shallow section and GC955 #001 deeper section.

Determination of pore pressure from the sonic log (PP_S) is based on the following equation:

$$PP_s = P_{ob} - (\frac{1}{\beta} ln \frac{\phi_o}{\phi}),$$

where β is a constant, ϕ_o is the initial porosity (at zero effective pressure in the mudline), ϕ is porosity derived from the compressional travel time:

$$\phi = 1 - (\frac{\Delta t_{ma}}{\Delta t})^{1/f},$$

where Δt is measured compressional travel time ($\Delta t = Vp^{-1}$, Vp is compressional-wave velocity), Δt_{ma} is the matrix travel time and f is an acoustic formation factor. β and ϕ_o were determined by Flemings et al. (2002) from the compaction trend of mudstone in the cores from Eugene Island 330 reservoirs (Gulf of Mexico), while f and Δt_{ma} were determined from the laboratory measurements in the same cores. However, all empirical constants used by Flemings et al. (2002) were defined for mudstone rock, thus may not provide completely accurate results for mud sediment section in our study area. We used analytical solution suggested by Flemings et al. (2002) to determine β and ϕ_o in our study area and values for f , Δt_{ma} based on Martin et al. (1988) and Zoback (2007) (see Table 1). We observed a good match (<1 MPa discrepancy) between our sonic-log-derived pore pressure and predicted hydrostatic pressure distribution in the upper sediment section (~0-300 mbsf (0-984 ftbsf)) as is expected for the shallow subseafloor sediments (Figure 3b). Additionally, our pore pressure calculations generally match the independent formation pressure measurements in the deeper sediment section in GC955 #001 well (Figure 3b). Therefore, we assume that our calculations provide sufficient accuracy for pore pressure prediction according to the objectives of the present study. All values used for the pore pressure calculations are included in Table 1.

According to Zhang (2011), Eaton's method of pore pressure prediction may be adapted using depth-dependent normal compaction trendline based on the case study in Green Canyon of the Gulf of Mexico (1520 m (4986 ft) water depth).

$$PP_{res} = P_{ov} - (P_{ob} - P_h)(\left(\frac{R}{R_o e^{\mathrm{bz}}}\right))^{\mathrm{n}} ,$$

where PP_{res} is pore pressure predicted from the resistivity log, R is measured resistivity at depth z. R_0 is resistivity near the mudline, b and n are the constant values, applicable for young sedimentary basins (Zhang, 2011) (Table 1).

4.2 Calculation of gas hydrate phase boundary

A theoretical hydrate stability phase diagram was generated using the CSMHYD program (Sloan and Koh, 2008), which uses an algorithm based on Gibbs energy minimization and accounts for variable pressure and temperature conditions, the composition of gas forming hydrates, and the presence of inhibitors of hydrate formation (e.g., salt). Assuming 99.9% methane gas and minimum and maximum measured pore water salinity of 17 and 35 ‰ (Flemings et al., 2018), CSMHYD program estimated the pressure at which hydrates are stable for any given temperature. The gas hydrate boundary was plotted in pressure-temperature coordinates against depth to compare with predicted pore pressure at various temperature gradients (Figure 3b, 5d).

4.3 Heat flow modeling

We use static finite-element models to study the thermomechanical effect of the GC955 diapir on its roof sediments and estimate the temperature at the hydrate reservoir (Figure 5). We run an axisymmetric model (Figure 5a) to capture the 3-dimensional nature of the diapir and we complement it with a plane-strain model to investigate the effect of non-circular, elongated sections of the salt (Figure 5b). In the axisymmetric model, the salt diapir is represented as axisymmetric salt dome. In the plane-strain model, the salt diapir is represented as a salt wall

extending perpendicular to the studied cross section with the same geometry. Basal heat flow is the only source of heat in the model, assuming that the radiogenic heat source is negligible compared to the basal heat flow. A uniform basal heat flow of 42 mW m^{-2} is applied across the base of the model (Christie and Nagihara, 2016) (Figure 5a, b). Heat conduction is the only mechanism of heat flow in the model. The thermal conductivity of sediments increases with depth following the trend suggested by Christie and Nagihara (2016) for sediments in the Gulf of Mexico. The thermal conductivity of salt is treated as a constant, 6.5 W m^{-1} K^{-1}, and specific heat capacity for salt and sediments is 860 J Kg^{-1} K^{-1} (Mello et al., 1995). Temperature at the seafloor is assumed to be 4 ^{o}C. The heat flow is assumed to have reached the equilibrium (steady) state.

5. Results

5.1 Pore pressure in the diapir roof sediments

We investigate whether anomalous pore pressure may be responsible for a ~400 m (1312 ft) discrepancy between the previously proposed base of GHSZ and its theoretical depth calculated based on the regional, average geothermal gradient in the area (Jones, 2003; Forrest et al., 2007). Standard gas hydrate phase boundary modeling a priori considers normal (hydrostatic) pore pressure gradient. However, the pore pressure may differ from hydrostatic pressure, especially in the Gulf of Mexico where rapid sedimentation drives high pore pressure and leads to wellbore instability and landslides (Flemings et al., 2008; Sawyer et al., 2009; Stigall and Dugan, 2010). In sediments above rising salt, pore pressure can also vary as described by Nikolinakou et al. (2018). As a salt diapir rises, the roof sediments undergo significant deformation and changes in both the mean and shear stress regimes, which may lead to overpressure or underpressure on the flanks and in the roof of the diapir (Nikolinakou et al., 2018).

To characterize the pore pressure within the diapir roof sediments in GC955, we combined LWD log data from Hole GC 955 H001 up to ~560 mbsf (1837 ftbsf), and GC955 #001 below 560

mbsf (1837 ftbsf) (Figure 3). To avoid misleading pore pressure values, we have excluded anomalously high velocity and resistivity measurements related to known gas hydrate bearing intervals and casing intervals (Figure 3c).

Figure 3b shows that pore pressure above the salt diapir in GC955 generally follows the normal hydrostatic trend down to ~1000 mbsf (3280 ftbsf), where it starts to increase and approaches the level of the overburden stress in proximity of the salt diapir. The overpressure increase is significantly below the hydrate reservoir depth (450 mbsf (1476 ftbsf)). This pattern is in a good agreement with the independent formation pressure measurements from the lower section of GC955 #001 well (Figure 3b). This pore pressure distribution is then coupled with a gas hydrate phase boundary diagram (CSMHYD, see methods), which considers the regional, average geothermal gradient for the Gulf of Mexico slope sediments (20°C/km) (6°C/1000 ft) (Jones, 2003; Forrest, 2007). Therefore, based on our pore pressure calculations, the modeled base of GHSZ is predicted at ~850 mbsf (2788 ftbsf) where the pore pressure point cloud intersects the GHSZ phase boundary (Figure 3b).

In contrast, previous studies suggest a much shallower depth for the base of GHSZ in the study area (~450 mbsf (1476 ftbsf)) based on the observation of the anomalous top of free gas at the GC 955 Q001 well (Boswell et al., 2012; Haines et al., 2017). In order to match this depth, pore pressure must be ≥15 MPa lower at the gas hydrate reservoir level (Figure 3b) which is not supported by the data.

5.2 Seismic evidence for lower base of GHSZ

Both 3D seismic data and high-resolution 2D seismic data at GC955 show high amplitude reflections below the previously assumed GHSZ lower boundary that have been interpreted to be gas (Shelander et al., 2012; Haines et al., 2017). At the same time, no clear BSR

has been presented in the GC955 study area thus far. Therefore, we consider an alternative scenario, in which the previously interpreted gas hydrate reservoir at 450 mbsf (1476 ftbsf) is located in the interior of GHSZ. In such a scenario, gas hydrate-related seismic indicators, normally observed at the base of GHSZ (BSR or enhanced seismic amplitudes) will be expected lower in the seismic section.

In our 3D seismic data, the coarse-grained gas hydrate reservoir appears at ~450 mbsf (1476 ftbsf) as a group of high-amplitude reflections, which can either have stratigraphic origin or be caused by the high acoustic impedance between water or gas and gas hydrate-bearing sediments (Figure 4a). Beyond that, deeper in the seismic data, another negative-polarity high-amplitude reflection occurs at ~750-850 mbsf (2460-2788 ftbsf) (300-400 m (984-1312 ft) below the upper gas hydrate reservoir) (Figure 4a). Root mean square (RMS) seismic amplitude maps for both upper and lower groups of reflections show general similarity in their spatial extent and structural layout in the arches of the multistage anticline framework (Figure 4b, c). RMS values of the lower group of reflections are generally 2x lower, however this may be a result of amplitude masking effect produced by the upper reservoir (Figure 4d). The lower group of reflections may be interpreted as free gas or the base of the GHSZ. Unfortunately, velocity log data from well GC955 #001, do not provide accurate acoustic velocities in the vicinity of the lower reservoir, because of the position of the casing during well logging (Figure 3c). However, available checkshot records for this well show distinct increase in the interval compressional velocity to 2100 m/s (6890 ft/s) for three individual shots at 2743-2971 mbsl (8113-9747 ftbsl), followed by a velocity drop to ~1800 m/s (~5905 ft/s) (Figure 3c) in the section below. The center of this interval agrees with both, the previously proposed theoretical base of GHSZ at 20 °C/km (6°C/1000 ft) geothermal gradient (~850 mbsf) (2788 ftbsf) (Figure 3b), and the depth

of the lower reservoir inferred from the 3D seismic data (Figure 4a). Therefore, check-shot interval velocity and positive polarity reflection in the seismic data are indicative of a deeper base of GHSZ in GC955 at ~750-850 mbsf (2460-2788 ftbsf). Poor seismic resolution at this depth and 76-m long check-shot intervals impede a more definitive estimate for the position of GHSZ base.

5.3 Modeling heat flow in the salt diapir roof

Another possible reason for the discrepancy in the GHSZ depth is a temperature anomaly resulting from the salt diapir. Thermal conductivity of salt bodies varies depending on the temperature (~7.2-4.0 W m^{-1} $°C^{-1}$ in 0-200°C interval) but remains very high compared to clastic sedimentary rocks (Mello et al., 1995). In contrast, mean thermal conductivity of clastic sedimentary rocks is several times lower (1.9-1.2 W m^{-1} k^{-1}) (Robertson, 1988; Mello et al., 1995). Therefore, salt diapirs behave as effective heat conductors, absorbing heat from the underlying and nearby sediment sections and channeling it upward to their roofs (Mello et al., 1995). Frye (2008) considered this effect on the regional scale for modeling the GHSZ in the northern Gulf of Mexico. This resulted in a notably thinner GHSZ over near-surface salt bodies. We conducted a similar heat flow modeling experiment but on a significantly finer scale to test the local effect of salt on temperature field in GC955. We applied a basal heat flow of 42 mW m^{-2} (Christie and Nagihara, 2016) at the bottom of 10x14 km 2D vertical section intersecting the central part of the salt diapir and location of well GC 955 H001 (Figure 2). Precise geometry of the salt diapir integrated in our heat flow model was derived from the 3D seismic data. These data constrained the distribution of thermal conductivity values – fundamental input parameter for the heat flow modeling – within our modeling domain. We ran two independent simulations - for axisymmetric (Figure 5a) and plane-strain (Figure 5b) model configurations. Because the salt diapir can be approximated as a dome (Figure 2b) the axisymmetric model better describes the 3-

dimensional salt geometry of the upper parts of the diapir. The plane-strain model (Figure 5b) better describes the in-plane salt geometry, but in essence simulates an infinitely long salt wall. We use the plane-strain results as an end member behavior that accounts for elongated salt sections in deeper parts of the salt body.

The axisymmetric model shows a strong positive temperature anomaly above the salt diapir (Figure 5a). In the upper ~500 m (1640 ft) of the salt roof, including the level of the gas hydrate reservoir (450 mbsf) (1476 ftbsf), the axisymmetric model suggests temperature gradient of 36-37 °C/km (11.3°C/1000 ft) (Figure 5c). Lower in the sediment section, it starts to continuously increase and reaches ~42 °C/km (~12.9°C/1000 ft) just above the top of the salt. The plane strain model shows very similar temperature gradient in the upper salt roof section (Figure 5c). We do observe some differences between the results of two models, particularly in the amount of heat flow above salt pedestal and around the central column (insets of Figures 5a,b), however this is significantly below the gas hydrate reservoir. At Hole GC 955 H001, temperature reaches ~21 °C at the gas hydrate reservoir level (red profiles on Figure 5c), which is only 1° lower than the maximum anomaly at the reservoir level right above the central diapir roof (blue profiles on Figure 5c). Therefore, the temperature at the gas hydrate reservoir is 8° C higher compared to the temperature predicted by regional, average geothermal gradient (Figure 5c). Nearest existing temperature gradient measurements, derived away from salt in GC955 #002 well, show even lower value (15.3 °C/km (4.6°C/1000 ft) in 2438-8046 mbsl (7998-26397 ftbsl) interval). However, these temperature measurements do not provide accurate geothermal gradient value, since they show annular temperature, affected by recycled drilling mud in the borehole. Using the model-predicted temperature gradient in the upper diapir roof (36 °C/km) (10.9 °C/1000 ft) and related temperature estimation for the reservoir level (21 °C) the theoretical hydrate stability

phase diagram predicts the base of stability at ~450-470 mbsf (1476-1541ftbsf), which matches well with the existing estimate for the base of GHSZ (Figure 5d).

6. Discussion

6.1 Evidence for shallow and deep base of GHSZ in GC955

The thickness of the GHSZ depends upon several major variables, including gas composition, pore pressure, pore water salinity, and geothermal gradient. In the GC955 study area, results of gas chromatographic (99.9% methane gas) and pore water salinity analyses (17-35 ‰) (Flemings et al., 2018) reduce the variables to pore pressure and geothermal gradient, which we determine with high confidence.

Herein, we considered two different possible depths for the base of GHSZ at GC955 (Figure 6). The first, shallower estimate at 450 mbsf (1476 ftbsf), and corresponding gas hydrate phase diagram require a high geothermal gradient above the salt diapir (36 °C/km) (10.9 °C/1000 ft) or a significant decrease in pore pressure (15 MPa) (Figure 3b). Our pore pressure calculations from both compressional velocity and resistivity logs show no deviation from the normal hydrostatic trend in the upper ~1000 mbsf (3280), thus we do not consider low pore pressure to be the cause of the shallow base of GHSZ. If a gradient of 36 °C/km (10.1°C/1000 ft) is invoked to explain the shallow base of the GHSZ, this means the gradient is significantly higher than regional geothermal gradient in the Green Canyon protraction area, which average 20 °C/km (6°C/1000 ft) (Jones, 2003; Forrest et al., 2007). This high gradient, however, has been well supported by the thermodynamic heat flow model applied in our study area (Figure 5).

The second hypothesis, where the base of the GHSZ occurs at ~750 mbsf (2460 ftbsf), allows for a lower geothermal gradient of ~20 °C/km (~6°C/1000 ft). This is supported by a strong negative peak amplitude in the 3D seismic data at 750 mbsf (2460 ftbsf) (Figure 4a) and high check-shot

velocity registered in this depth interval, which implies a potential gas hydrate overlying a free gas accumulation. However, given the observation of gas below the gas hydrate interval at 442 mbsf in GC 955 Q001 well (Collett et al., 2012; Haines et al., 2017) (Figure 1), confirmed by strong negative peak amplitudes (Figure 3a, 4a), and the apparent salt control on the heat flow redistribution (Figure 5), we consider it the less likely hypothesis.

Even with a high modeled temperature gradient (36 °C/km) (10.1 °C/1000 ft), there is a possibility of structure II (which includes methane and heavier order hydrocarbons) gas hydrate formation beneath the documented structure I (almost pure methane) hydrate reservoir, as was the case of the deeper thermogenic gas infiltration shown by Paganoni et al. (2016) for offshore NW Borneo. Yet, gas hydrate phase boundary modeling shows that methane concentration even as low as 70% of the bulk gas composition, only results in the base of GHSZ at ~570 mbsf (1870 ftbsf), which is significantly above the strong negative peak amplitude observed in the 3D seismic data at ~750 mbsf (2460 ftbsf). Instead, we infer that the lower reservoir accommodates free gas accumulation possibly attributed to sandy or silty levee deposits related to a channel system farther to the east. Potentially, this reservoir may be an important component of the GC955 fluid flow system, supplying methane gas towards the bottom of GHSZ along the diapir-roof fault system, interpreted in the seismic data (Figure 4a). Although pore pressure analysis shows no deviation from the normal hydrostatic trend at the GHSZ lower boundary, it shows an apparent increase in the lower ~500 m (1640 ft) of the diapir-roof sediment section. Such observations conform to existing modeling of stress and pressure regimes around salt diapirs (Nikolinakou et al., 2018) and may be critical in similar gas hydrate systems with thinner diapir roofs, where disturbed stress field is able to reach the GHSZ.

6.2 Evolution of the GHSZ above salt diapirs

Our analysis indicates that temperature anomalies can be caused by an underlying salt diapir, which likely exert a fundamental control on the life cycle of the gas hydrate reservoir in GC955. Salt diapirs progress upward driven by sediment loading and tectonic forces (Jackson and Hudec, 2017). At the later stages of diapir development, the salt relative rise rate may override the sedimentation rate (Nikolinakou et al., 2017), accelerating the diapir approach to the seafloor. Numerical studies have also shown that diapirs can upbuild through thick roofs, when such roofs consist of highly plastic marine muds and mudrocks (Nikolinakou et al., 2017). This upbuilding results in anticlinal doming and emergence of structural traps for gas hydrate above the base of the GHSZ and natural gas reservoirs below. Importantly, salt upbuilding also shallows the base of the GHSZ by channeling heat upward. Therefore, it is reasonable to assume that the present day configuration of GHSZ in GC955 may continue to thin with future salt diapir growth.

Based on our study, we propose a generalized mechanism for a long-term evolution of similar gas hydrate systems, governed by a salt diapir initiation and growth. In a hypothetical scenario with no salt involved, the relative location of the base of the GHSZ will remain at the same distance from the seafloor, but will transition through the sedimentary section as new sediment is deposited and buried. Such a process can result in continuous recycling between gas and gas hydrate at the base of GHSZ as shown by Burwicz et al. (2017), yet the relative GHSZ thickness will remain constant. On the contrary, if a salt diapir rises from below, a temperature-related warping of the GHSZ will superimpose upon this uniform shift pattern (Figure 7). Given that our thermodynamic modeling shows robust correlation between the temperature gradient and distance to the top of a diapir (Figure 5), salt upbuilding would inevitably lead to continuously increasing temperature in the diapir roof as it progresses upward. This process will facilitate

contraction of GHSZ, eventually pierce it, and accelerate the dissociation of any gas hydrate reservoir (figure 7).

Therefore, we propose the following generalized model for a gas hydrate reservoir above a rising salt diapir: 1. A rising salt diapir creates a structural framework, favorable for accumulation of gas and gas hydrate at the base of GHSZ due to creation of anticlinal traps and potential fluid advection through the faults; 2. A salt-induced increase in the temperature gradient shifts the base of GHSZ upward. Elevated pore pressure is not yet affecting the GHSZ at this time; 3. Increasing pore pressure above the salt diapir and extensional stress regime support fluid flow and gas transport through the thinned GHSZ towards the seafloor. Increase in temperature gradient continues as salt rises; 4. If any gas hydrate reservoir has formed above the salt diapir, it will eventually become thermodynamically unstable if the salt top approaches close to the seafloor (Figure 7). This general mechanism may apply for characterization of similar gas hydrate reservoirs in other marine salt tectonic provinces along the continental margins, where gas hydrate is thermodynamically stable (Figure 1). Technically, such salt-induced collapse of gas hydrate reservoirs is similar to the dissociation of methane hydrate above salt diapirs across the shallow Gulf of Mexico shelf (<400 mbsl (1312 ftbsl)), driven by reciprocal migration of gas hydrate stability field during Pleistocene sea level fluctuations (±120 m) (±393 ft) (Roberts and Carney, 1997).

Evidence for the ultimate dissociation of diapir-roof gas hydrate reservoirs is visible in the newly released high-resolution bathymetry data in the other regions of deep-water Gulf of Mexico (Kramer and Shedd, 2017), where gas hydrates are inferred to be thermodynamically stable assuming regional, average geothermal gradient. There, abundant fields of pockmarks and possibly mud volcanoes appear at the seafloor above many thin roofed (<700 m) (<2296 ft) salt

diapirs (Figure 8). Here, we demonstrate the shaded seafloor slope maps above salt diapirs with different roof sediment thicknesses, and possible indications of gas and gas hydrate accumulations. Figure 8a demonstrates a salt diapir with overlying high amplitude reflections in Keathley Canyon, 1750 m (5441 ft) water depth. Similar to GC955 scenario, this may indicate gas or gas hydrate accumulation in the salt roof. Yet, the roof of this diapir is 2x thinner (~680 m) (2230 ft) compared to the GC955 diapir and has apparent seafloor expression with several pockmarks in the high-resolution seafloor slope data (Figure 8a). Therefore, we assume that this diapir-roof system belongs between stage 2 and early stage 3 according to our generalized model.

Figures 8b and 8c show examples of two salt diapirs from Keathley Canyon and Garden Banks respectively, with abundant pockmarks on the seafloor above them. Figure 8c shows a prominent BSR at ~150 mbsf (492 ftbsl), indicating a shallow base of GHSZ overlying the salt diapir. We suggest these demonstrated salt diapir systems belong to stage 3 or early stage 4 in our model classification. Finally, figure 8d shows a salt diapir in Walker Ridge, which outcrops at the seafloor. A discontinuous BSR extends above the flank of the diapir, approaches close to the seafloor as the salt top becomes shallower, and finally merges with the seafloor reflector close to where salt outcrops at the surface (Figure 8d). Such BSR behavior indicates increasing temperature effect close to the heat-conductive salt diapir, which is in a good agreement with our heat flow numerical model (Figure 5). We do not observe any fluid flow features on the seafloor, likely because the outcropping salt has significantly affected the seafloor morphology. Such a salt diapir system represents late stage 4 in our model.

Upward gas transport expressed in the seafloor morphology may be additionally supported by the opening systems of normal faults in the established regime of extensional stress, typical for

diapir roof sediments (Jackson and Talbot, 1986) (Figures 4a). Even in the GC955 area with a thick diapir roof, several gas flares in the water column, and possibly a mud volcano, have already been observed above a deep-seated fault reaching the seafloor (Figure 2) (Heggland, 2004; National Geophysical Data Center, 2012). Although at present we do not observe increased pore pressure and pore water salinity as deep as 450 mbsf (1476 ftbsf) in Hole GC955 H005 (Flemings et al., 2018) or pore pressure increases in the nearby industry well GC955 #001, this is expected to occur at the latter stages of salt diapir growth (Bruno and Hanor, 2003; Nikolinakou et al., 2017; Nikolinakou et al., 2018). Indeed, pore pressure modeling in GC955 does show notable increase in the pore pressure trend in the lower section of the diapir roof, proximal to the top of salt (Figure 3b). Although it requires further subject-oriented studies, abnormal pressure and elevated pore-water salinity at the base of GHSZ may provide additional constraints for gas hydrate modeling and need to be accounted in such dynamic geological systems.

7. Conclusions

Pore pressure reconstructions based on the well log data in GC955 do not indicate any major over- or under-pressure in the upper 1000 m (3280 ft) of the salt diapir roof. Instead, finite-element heat flow models show that conductive salt body produces a significant temperature anomaly, reaching 8 °C at the gas hydrate reservoir level. Such salt-induced temperature anomaly shifts the base of the GHSZ by as much as 400 m (1312 ft) above the depth based on a regional, average temperature gradient for Green Canyon, Gulf of Mexico (20 °C/km) (6°C/1000 ft). Based on the existing salt diapir evolution models, we propose the generalized mechanism for initiation and collapse of salt-driven gas hydrate reservoirs in the Gulf of Mexico and similar salt provinces worldwide. Such mechanism is well supported by multiple pockmark fields and

mud volcanoes observed in the bathymetry data over a range of diapir-roof gas hydrate systems in several locations across the deep-sea Gulf of Mexico.

8. Disclaimer

This material is based upon work supported by the Department of Energy under Award Number and DE-FE0023919. This report was prepared as an account of work sponsored by an agency of the United States Government. Neither the United States Government nor any agency thereof, nor any of their employees, makes any warranty, express or implied, or assumes any legal liability or responsibility for the accuracy, completeness, or usefulness of any information, apparatus, product, or process disclosed, or represents that its use would not infringe on privately owned rights. Reference herein to any specific commercial product, process, or service by trade name, trademark, manufacturer, or otherwise does not necessarily constitute or imply its endorsement, recommendation, or favoring by the United States Government or any agency thereof. The views and opinions of authors expressed herein to not necessarily state or reflect those of the United States Government or any agency thereof.

9. References

Boswell, R., T. S. Collett, M. Frye, W. Shedd, D. R. McConnell, and D. Shelander, 2012, Subsurface gas hydrates in the northern Gulf of Mexico: Marine and Petroleum Geology, v. 34, p. 4-30.https://doi.org/10.1016/j.marpetgeo.2011.10.003

Bruno, R. S., and J. S. Hanor, 2003, Large-scale fluid migration driven by salt dissolution, Bay Marchand dome, offshore Louisiana: Gulf Coast Association of Geological Societies Transactions, v. 53, p. 97-107

Burwicz, E., T. Reichel, K. Wallmann, W. Rottke, M. Haeckel, and C. Hensen, 2017, 3-D basin-scale reconstruction of natural gas hydrate system of the Green Canyon, Gulf of Mexico: Geochemistry, Geophysics, Geosystems, v. 18, p. 1959-1985.doi:10.1002/2017GC006876

Christie, C. H., and S. Nagihara, 2016, Geothermal gradients of the northern continental shelf of the Gulf of Mexico: Geosphere, v. 12, p. 26-34.10.1130/GES01163.1

Collett, T., 2002, Energy Resource Potential of Natural Gas Hydrates: AAPG Bulletin, v. 86, p. 1971-1992.10.1306/61EEDDD2-173E-11D7-8645000102C1865D

Collett, T. S., M. W. Lee, M. V. Zyrianova, S. A. Mrozewski, G. Guerin, A. E. Cook, and D. S. Goldberg, 2012, Gulf of Mexico Gas Hydrate Joint Industry Project Leg II logging-while-drilling data acquisition and analysis: Marine and Petroleum Geology, v. 34, p. 41-61.https://doi.org/10.1016/j.marpetgeo.2011.08.003

Diegel, F. A., J. F. Karlo, D. C. Schuster, R. C. Shoup, and P. R. Tauvers, 1995, Cenozoic structural evolution and tectono-stratigraphic framework of the northern Gulf coast continental margin: M. P. A. Jackson, D. G. Roberts, and S. Snelson, eds., Salt tectonics: a global perspective: AAPG, v. 65, p. 109-151

Flemings, P. B., H. Long, B. Dugan, J. Germaine, C. M. John, J. H. Behrmann, D. Sawyer, and I. E. Scientists, 2008, Pore pressure penetrometers document high overpressure near the seafloor where multiple submarine landslides have occurred on the continental slope, offshore Louisiana, Gulf of Mexico: Earth and Planetary Science Letters, v. 269, p. 309-325.https://doi.org/10.1016/j.epsl.2007.12.005

Flemings, P. B., S. Phillips, C, T. Collett, A. Cook, R. Boswell, and U.-G. E. Scientists, 2018, Hydrate Pressure Coring Expedition Report: Austin, TX University of Texas Institute for Geophysics, TX.

Flemings, P. B., B. B. Stump, T. Finkbeiner, and M. Zoback, 2002, Flow focusing in overpressured sandstones: Theory, observations, and applications: American Journal of Science, v. 302, p. 827-855.10.2475/ajs.302.10.827

Forrest, J., E. Marcucci, and P. Scott, 2007, Geothermal gradients and subsurface temperatures in the northern Gulf of Mexico: Gulf coast Association of Geologica; Societies Transactions, v. 55, p. 233-248

Frye, M., 2008, Preliminary Evaluation of In-Place Gas Hydrate Resources: Gulf of Mexico Outer Continental Shelf, *in* M. Frye, ed., Minerals Management Service report 2008-004.

Haacke, R. R., G. K. Westbrook, and R. D. Hyndman, 2007, Gas hydrate, fluid flow and free gas: Formation of the bottom-simulating reflector: Earth and Planetary Science Letters, v. 261, p. 407-420.https://doi.org/10.1016/j.epsl.2007.07.008

Haines, S. S., P. E. Hart, T. S. Collett, W. Shedd, M. Frye, P. Weimer, and R. Boswell, 2017, High-resolution seismic characterization of the gas and gas hydrate system at Green Canyon 955, Gulf of Mexico, USA: Marine and Petroleum Geology, v. 82, p. 220-237.https://doi.org/10.1016/j.marpetgeo.2017.01.029

Heggland, R., 2004, Definition of geohazards in exploration 3-D seismic data using attributes and neural-network analysis: AAPG Bulletin, v. 88, p. 857-868.10.1306/02042004

Jackson, M. P. A., and M. R. Hudec, 2017, Salt Tectonics: Principles and Practice: Cambridge, Cambridge University Press, 498 p.

Jackson, M. P. A., and C. J. Talbot, 1986, External shapes, strain rates, and dynamics of salt structures: GSA Bulletin, v. 97, p. 305-323.10.1130/0016-7606(1986)97<305:ESSRAD>2.0.CO;2

Jones, M. L., 2003, The regional geothermal heat flow regime of the north-central Gulf of Mexico continental slope, Texas Tech University, Texas Tech University, 136 p.

Kinoshita, M., G. F. Moore, and Y. N. Kido, 2011, Heat flow estimated from BSR and IODP borehole data: Implication of recent uplift and erosion of the imbricate thrust zone in the Nankai Trough off Kumano: Geochemistry, Geophysics, Geosystems, v. 12.10.1029/2011GC003609

Kramer, K. V., and W. W. Shedd, 2017, A 1.4-billion-pixel map of the Gulf of Mexico seafloor: Earth and Space Science News, v. 98

Kvenvolden, K. A., and T. D. Lorenson, 2001, The Global Occurrence of Natural Gas Hydrate, Natural Gas Hydrates: Occurrence, Distribution, and Detection, American Geophysical Union, p. 3-18.

McConnell, D. R., 2000, Optimizing Deepwater Well Locations To Reduce the Risk of Shallow-Water-Flow Using High-Resolution 2D and 3D Seismic Data, Offshore Technology Conference, Houston, Texas, Offshore Technology Conference.

McConnell, D. R., T. S. Collett, R. Boswell, M. Frye, W. W. Shedd, R. S. Dufrene, P. D. Godfriaux, S. Mrozewski, G. Guerin, A. Cook, and E. Jones, 2010, Gulf of Mexico Gas Hydrate Joint Industry Project Leg II: Initial Results from the Green Canyon 955 Site, Offshore Technology Conference, Houston, Texas, USA, Offshore Technology Conference, p. 14.

McConnell, D. R., Z. Zhang, and R. Boswell, 2012, Review of progress in evaluating gas hydrate drilling hazards: Marine and Petroleum Geology, v. 34, p. 209-223.https://doi.org/10.1016/j.marpetgeo.2012.02.010

McIver, R. D., 1982, Role of Naturally Occurring Gas Hydrates in Sediment Transport: AAPG Bulletin, v. 66, p. 789-792

Mello, U. T., G. D. Karner, and R. N. Anderson, 1995, Role of salt in restraining the maturation of subsalt source rocks: Marine and Petroleum Geology, v. 12, p. 697-716.https://doi.org/10.1016/0264-8172(95)93596-V

National Geophysical Data Center, N., 2012, NOAA Office of Ocean Exploration and Research (2012): Water Column Sonar Data Collection (EX1202L3, EM302), *in* N. National Centers for Environmental Information, NOAA, U.S. Department of Commerce, ed.

Nikolinakou, M. A., M. Heidari, P. B. Flemings, and M. R. Hudec, 2018, Geomechanical modeling of pore pressure in evolving salt systems: Marine and Petroleum Geology, v. 93, p. 272-286.https://doi.org/10.1016/j.marpetgeo.2018.03.013

Nikolinakou, M. A., M. Heidari, M. R. Hudec, and P. B. Flemings, 2017, Initiation and growth of salt diapirs in tectonically stable settings: Upbuilding and megaflaps: AAPG Bulletin, v. 101, p. 887-905.10.1306/09021615245

Paganoni, M., J. A. Cartwright, M. Foschi, R. C. Shipp, and P. Van Rensbergen, 2016, Structure II gas hydrates found below the bottom-simulating reflector: Geophysical Research Letters, v. 43, p. 5696-5706.10.1002/2016GL069452

Peel, F. J., C. J. Travis, and J. R. Hossack, 1995, Genetic Structural Provinces and Salt Tectonics of the Cenozoic Offshore U.S. Gulf of Mexico: A Preliminary Analysis, *in* M. P. A. Jackson, D. G. Roberts, and S. Snelson, eds., Salt Tectonics: A Global Perspective, American Association of Petroleum Geologists, p. 153-175.

Phrampus, B. J., R. N. Harris, and A. M. Tréhu, 2017, Heat flow bounds over the Cascadia margin derived from bottom simulating reflectors and implications for thermal models of subduction: Geochemistry, Geophysics, Geosystems, v. 18, p. 3309-3326.doi:10.1002/2017GC007077

Portnov, A., S. Vadakkepuliyambatta, J. Mienert, and A. Hubbard, 2016, Ice-sheet-driven methane storage and release in the Arctic: Nature Communications, v. 7.10.1038/ncomms10314

Roberts, H. H., and R. S. Carney, 1997, Evidence of episodic fluid, gas, and sediment venting on the northern Gulf of Mexico continental slope: Economic Geology, v. 92, p. 863-879.10.2113/gsecongeo.92.7-8.863

Robertson, E. C., 1988, Thermal properties of rocks, *in* U. S. G. Survey, ed., Open-file report 88-441, Denver, Colorado, U.S. Dept. of the Interior, Geological Survey p. 106.

Ruppel, C., G. R. Dickens, D. G. Castellini, W. Gilhooly, and D. Lizarralde, 2005, Heat and salt inhibition of gas hydrate formation in the northern Gulf of Mexico: Geophysical Research Letters, v. 32.doi:10.1029/2004GL021909

Sawyer, D. E., P. B. Flemings, B. Dugan, and J. T. Germaine, 2009, Retrogressive failures recorded in mass transport deposits in the Ursa Basin, Northern Gulf of Mexico: Journal of Geophysical Research: Solid Earth, v. 114.10.1029/2008JB006159

Shedd, W., R. Boswell, M. Frye, P. Godfriaux, and K. Kramer, 2012, Occurrence and nature of “bottom simulating reflectors” in the northern Gulf of Mexico: Marine and Petroleum Geology, v. 34, p. 31-40.https://doi.org/10.1016/j.marpetgeo.2011.08.005

Shelander, D., J. Dai, G. Bunge, S. Singh, M. Eissa, and K. Fisher, 2012, Estimating saturation of gas hydrates using conventional 3D seismic data, Gulf of Mexico Joint Industry Project Leg II: Marine and Petroleum Geology, v. 34, p. 96-110.https://doi.org/10.1016/j.marpetgeo.2011.09.006

Sloan, E. D., and C. A. Koh, 2008, Clathrate Hydrates of Natural Gases, Third Edition: Clathrate Hydrates of Natural Gases, Third Edition, CRC Press, 752 p.

Stigall, J., and B. Dugan, 2010, Overpressure and earthquake initiated slope failure in the Ursa region, northern Gulf of Mexico: Journal of Geophysical Research: Solid Earth, v. 115.doi:10.1029/2009JB006848

Wood, W. T., J. F. Gettrust, N. R. Chapman, G. D. Spence, and R. D. Hyndman, 2002, Decreased stability of methane hydrates in marine sediments owing to phase-boundary roughness: Nature, v. 420, p. 656.10.1038/nature01263

Wood, W. T., and C. Ruppel, 2000, Seismic and thermal investigations of the Blake Ridge gas hydrate area: a synthesis, *in* C. Paull, R. Matsumoto, P. J. Wallace, and W. P. Dillon, eds., Proceedings of the Ocean Drilling Program, Scientific Results, Vol 164, p. 253-264.

Worrall, D. M., and S. Snelson, 1989, Evolution of the northern Gulf of Mexico, with emphasis on Cenozoic growth faulting and the role of salt, *in* A. W. Bally, and A. R. Palmer, eds., The Geology of North America—An Overview, Geological Society of America, p. 97-138.

Zhang, J., 2011, Pore pressure prediction from well logs: Methods, modifications, and new approaches: Earth-Science Reviews, v. 108, p. 50-63.https://doi.org/10.1016/j.earscirev.2011.06.001

Zoback, M. D., 2007, Reservoir Geomechanics: Cambridge, Cambridge University Press, 449 p.

VITA

Alexey Portnov is a postdoc with The Ohio State University School of Earth Sciences. He received his PhD in marine geophysics in 2015 in the Center for Arctic Gas Hydrate Environment and Climate in The Arctic University of Norway. Alexey's research focuses on gas and gas hydrate reservoirs in dynamic geological systems including permafrost, glaciated continental margins and active salt tectonics regions.

Ann E. Cook is an associate professor in the School of Earth Sciences at The Ohio State University in Columbus, Ohio. She is interested in gas hydrate systems, especially petrophysics and remote detection. Her PhD is from Columbia University in New York.

Mahdi Heidari received his Ph.D. in geotechnical engineering from The University of Texas at Austin (UT-Austin) in 2013 and is currently a research associate at the Bureau of Economic Geology, UT-Austin. His research is focused on using geomechanical and seismic models to predict pore pressure, stress, and temperature in evolving salt systems.

Derek E. Sawyer is an assistant professor with The Ohio State University School of Earth Sciences. He received his B.S. degree in marine science from Eckerd College, M.S. degree in geosciences from Penn State University, and Ph.D. degree from the University of Texas at Austin. His research focus is on sedimentary transport processes in modern and ancient basins.

Manasij Santra is a postdoctoral fellow at the Institute for Geophysics, The University of Texas at Austin. His interests include clastic depositional processes and architecture of clastic deposits with special focus on marine gas hydrate reservoirs. Manasij has worked for ConocoPhillips and Reliance Industries. He received his PhD from The University of Texas at Austin, and MSc from IIT, Kharagpur.

Maria Nikolinakou is research scientist at the Bureau of Economic Geology, The University of Texas at Austin. Previously, she worked for Shell E&P. She received her M.Sc. and Sc.D. on theoretical soil mechanics from Massachusetts Institute of Technology and Diploma in Civil Engineering from National Technical University of Athens, Greece. She studies geomechanical stress and pressure in evolving geologic systems.

Figure captions

Figure 1. Red polygons indicate major known marine salt basins on Earth. Modified from Jackson and Talbot (1992).

Figure 2. a) Shaded relief map (Kramer and Shedd, 2017) and 3D seismic-derived bathymetry (blocks GC955, GC956, GC998, GC999, GC1000 of Green Canyon protraction area). Inset shows the location of the study area in the northern Gulf of Mexico. Wells are marked with yellow circles and labeled. Location of the inset in Figure 2b is marked with the red box. b) Map showing the top-salt surface depth in our study area meters below sea level (mbsl), outline of the gas hydrate reservoir (semi-transparent red area) and location of the seismic lines and modeling section, shown in Figures 3, 4 and 5.

Figure 3. a) Seismic section a-b crossing the central part of the diapir roof sediment section (location of the line is shown in Figure 2b) and two wells GC 955 H001 and GC955 #001. Dashed boxes indicate log intervals used for pore pressure predictions in each well. b) Pore pressure prediction from the compressional velocity and resistivity logs in the diapir roof sediment section, coupled with gas hydrate stability zone (GHSZ) phase boundary diagram (at 20 °C/km regional, average geothermal gradient) (Jones, 2003; Forrest et al., 2007) show a ~400 m (1312 ft) deeper theoretical base of GHSZ compared with its existing estimate (Boswell et al., 2012; Haines et al., 2017). c) Compressional velocity logs used for pore pressure prediction from wells GC 955 H001 and GC955 #001, showing anomalous velocity within the gas hydrate and casing intervals, which were excluded from our calculations. Check-shot interval velocity from well GC955 #001 is shown in brown.

Figure 4. a) 3D seismic image of the diapir roof sediment section, showing the upper gas hydrate reservoir and the lower reservoir that could be gas or hydrate. Black lines mark major faults cutting both reservoirs. Location of the inline and crossline is indicated in Figure 2b and Figure 4b, c. b) root mean square (RMS) seismic amplitude map for the depth interval b (indicated in Figure 4a) showing the configuration of the upper gas hydrate reservoir. Dashed white line is the superimposed outline of the lower reservoir c) RMS seismic amplitude map for the depth interval c (indicated in Figure 4a) showing the configuration of the lower reservoir. Dashed white line is the superimposed outline of the upper gas hydrate reservoir. d) Example of the seismic energy absorption by the upper gas hydrate reservoir along three inlines extracted from "sweetness" attribute volume in the area marked with yellow box in Figure 4b,c. Sweetness is derived by dividing instantaneous amplitude by the square root of instantaneous frequency.

Figure 5. Heat flow numerical simulations in the GC955 study area show significantly higher geothermal temperatures above the crest of the salt diapir compared to its margins: a) the axisymmetric model and b) the plane-strain model. The location of a 14 km (8.7 mi) deep cross section c-d, used in the numerical model is shown in Figure 2. Insets show the entire modeled salt cross section. Note the different color scale between the insets and zoomed-in salt roof sections. c) Temperature gradients (t_{grad}) along two probe sites (GC 955 H001 well location (red) and maximum observed anomaly (blue) for comparison). Solid lines show axisymmetric results and dashed lines show plane-strain results. d) Coupled pore pressure and gas hydrate phase boundary modeling modulated by the updated temperature gradient (36 °C/km) shows good agreement with the existing estimate for the base of gas hydrate stability zone (GHSZ). bsl = below sea level.

Figure 6. Possible scenarios supporting shallow and deep gas hydrate stability zone (GHSZ) base in GC955. Structure II gas hydrate in the deep (750 mbsf, 2460 ftbsf) scenario implies higher content of heavier order hydrocarbons in the total gas composition compared to structure I (almost pure methane).

Figure 7. Diagram showing major stages of a salt diapir-controlled gas hydrate reservoir evolution from its initiation to ultimate collapse. GHSZ = gas hydrate stability zone. T_{grad} = temperature gradient.

Figure 8. Examples of pockmark fields and shallow Bottom Simulating Reflections (BSRs) above the salt diapirs in Keathley Canyon, Garden Banks and Walker Ridge in the deep water Gulf of Mexico (>1100 mbsl [meters below sea level]) (>3608 ftbsl [feet below sea level]). Demonstrated examples belong to stages 2-4 according to our model (Figure 7). Yellow lines on the shaded slope bathymetry plots show location of the related seismic sections below.

Tables

Table 1 – calculated, measured parameters and constants, used for the pore pressure predictions.

Calculated parameters		Measured parameters	
P_h	hydrostatic pressure (Pa)	h_w	water depth (m)
P_{ob}	overburden pressure (Pa)	h	total depth (m)
PP_s	pore pressure from sonic log (Pa)	Δt	acoustic slowness (µs m^{-1})
PP_{res}	pore pressure from resistivity log (Pa)	R	resistivity (ohm m)
ϕ	porosity	ρ_b	bulk density (kg m^{-3})
Constants			
ρ_w	water density (kg m^{-3})		1024
g	acceleration for gravity (m s^{-2})		9.81
f	acoustic formation factor (-)		2.1
Δt_{ma}	matrix travel time (µs m^{-1})		56
β	beta-constant (MPa^{-1})		0.063
φ_0	initial porosity		0.487
R_0	compaction resistivity in the mudline (Ω m)		1
b	constant (-)		3.4×10^{-5}
n	exponent (-)		1.2

indicated values are applicable for young sedimentary basins

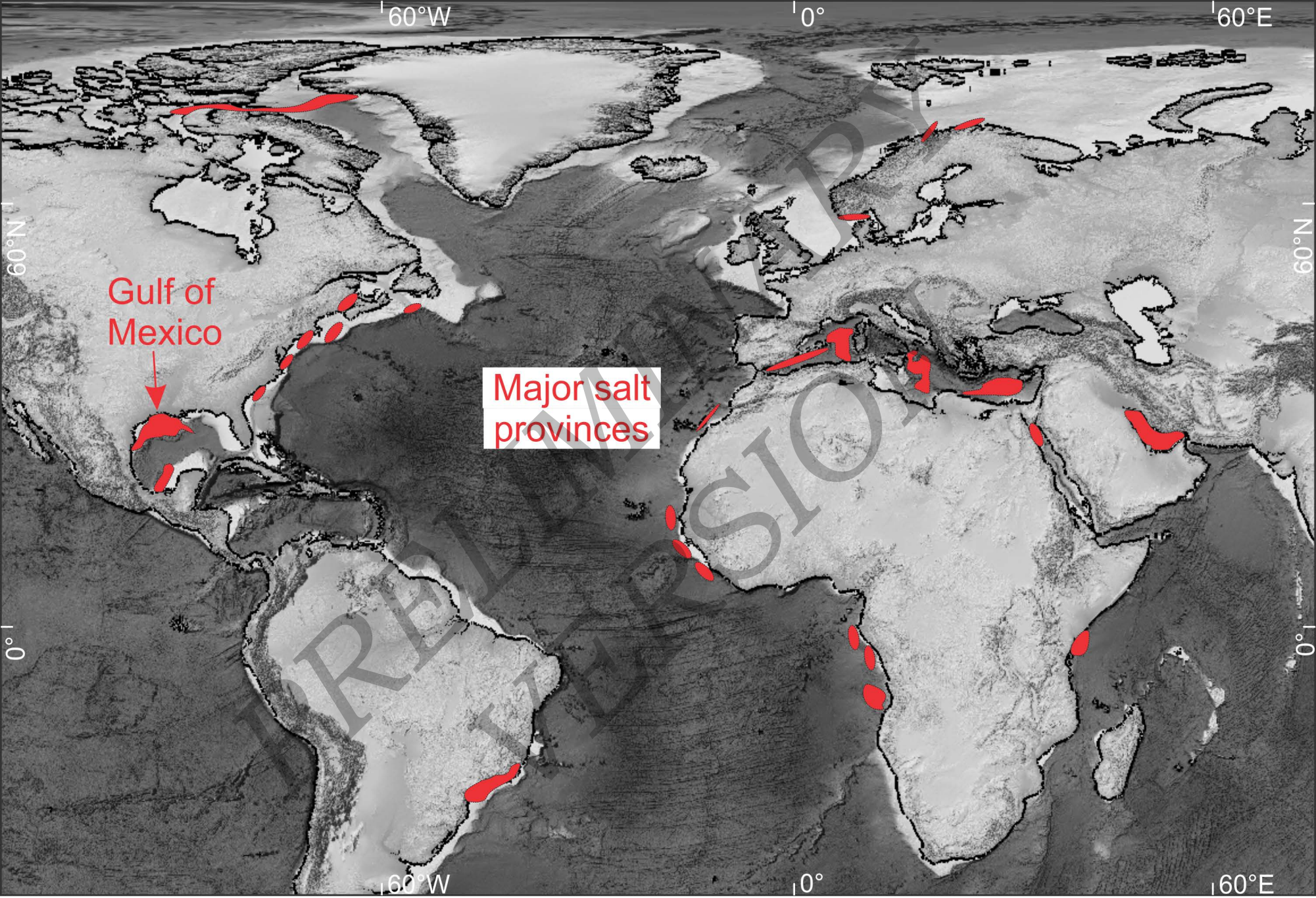
60°W
0°
60°E
60°N
0°
Gulf of Mexico
Major salt provinces
PRELIMINARY VERSION

Figure 1

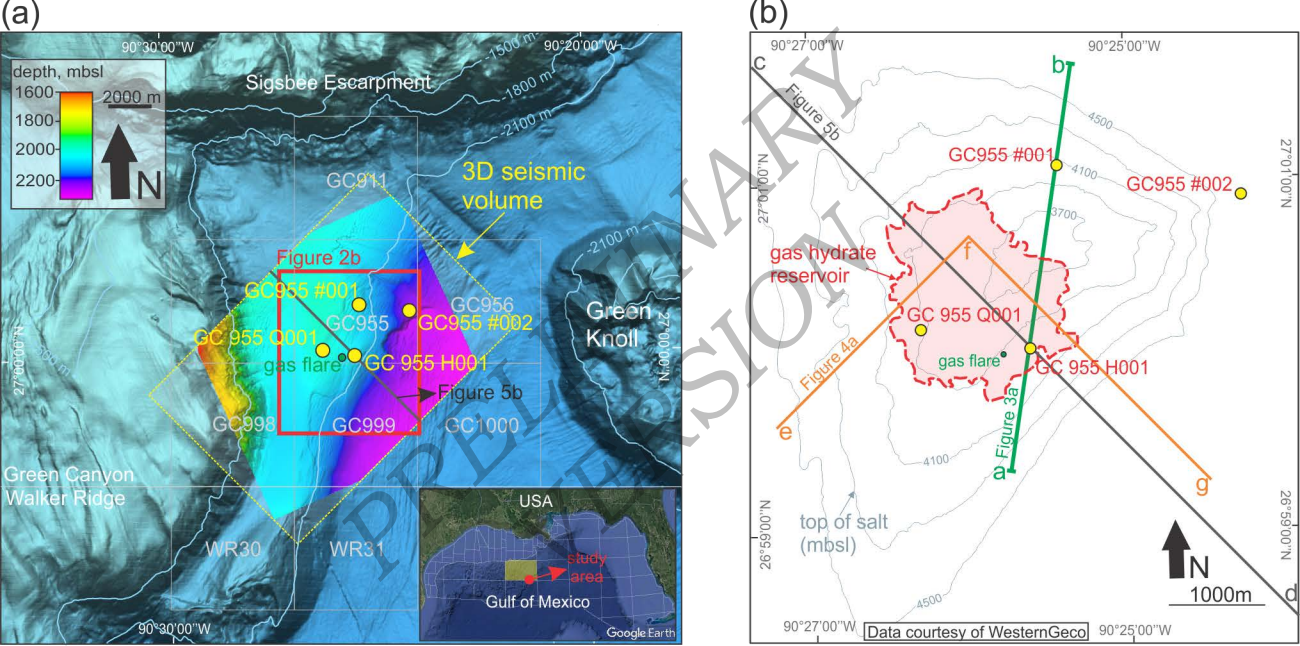

Figure 2

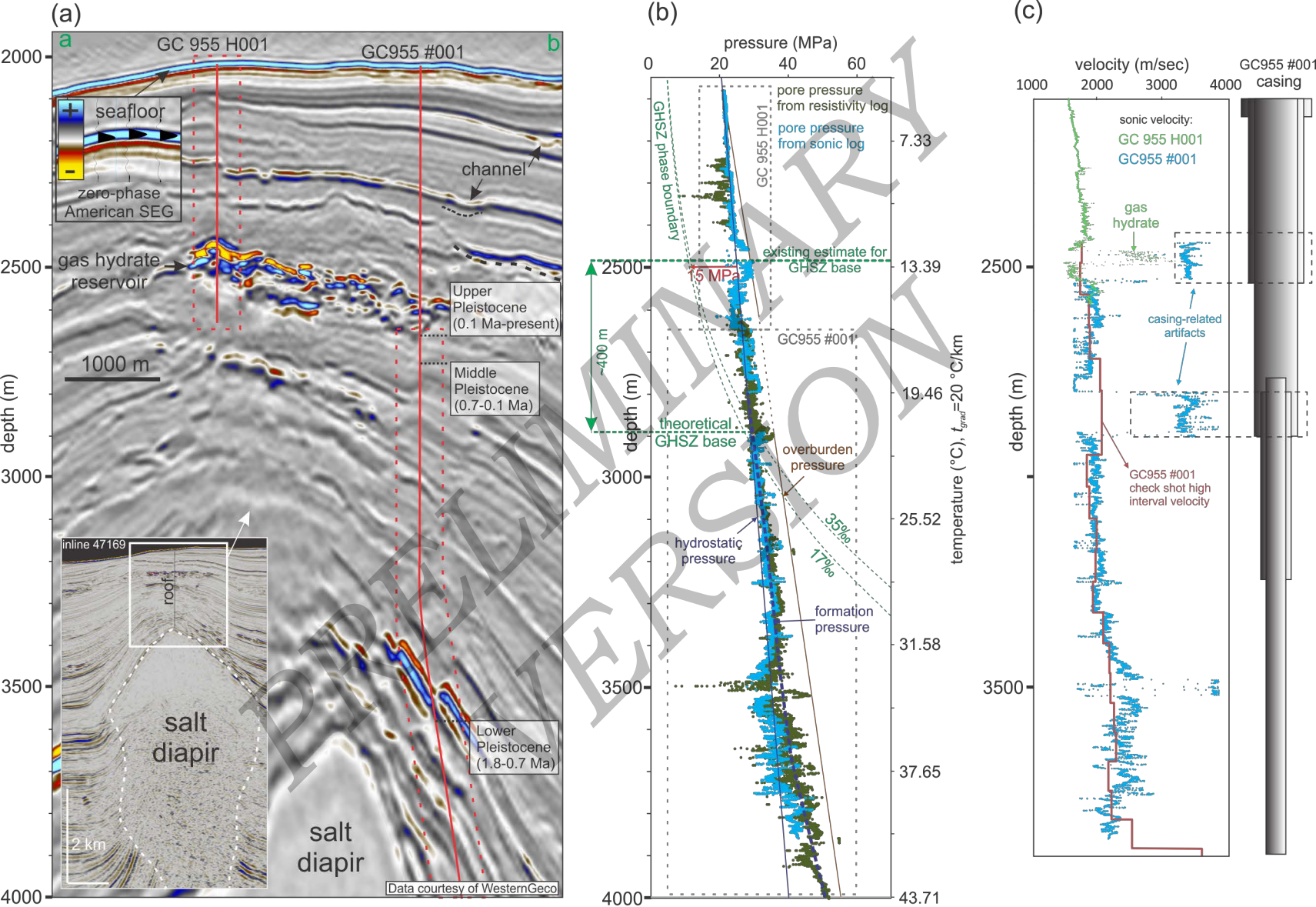

Figure 3

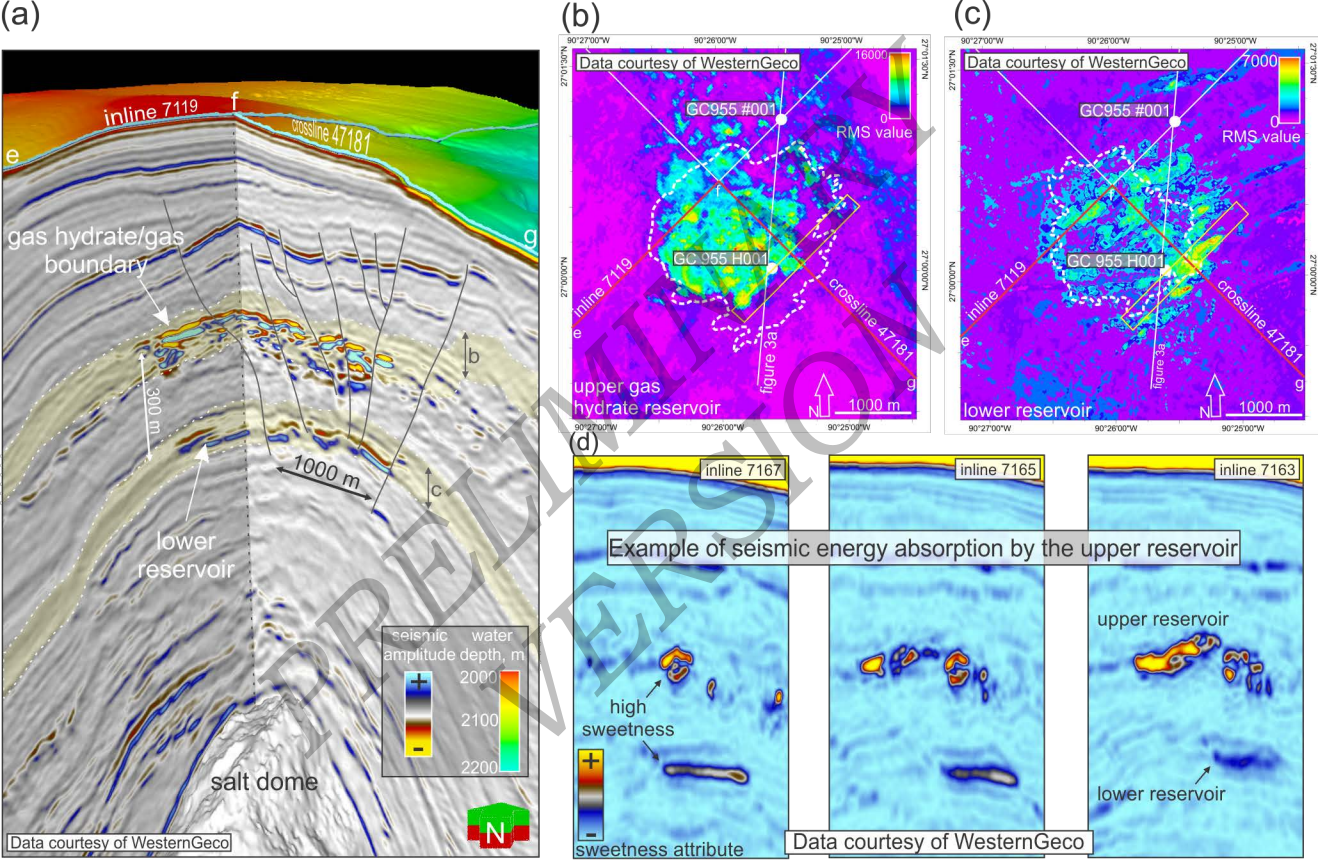

Figure 4

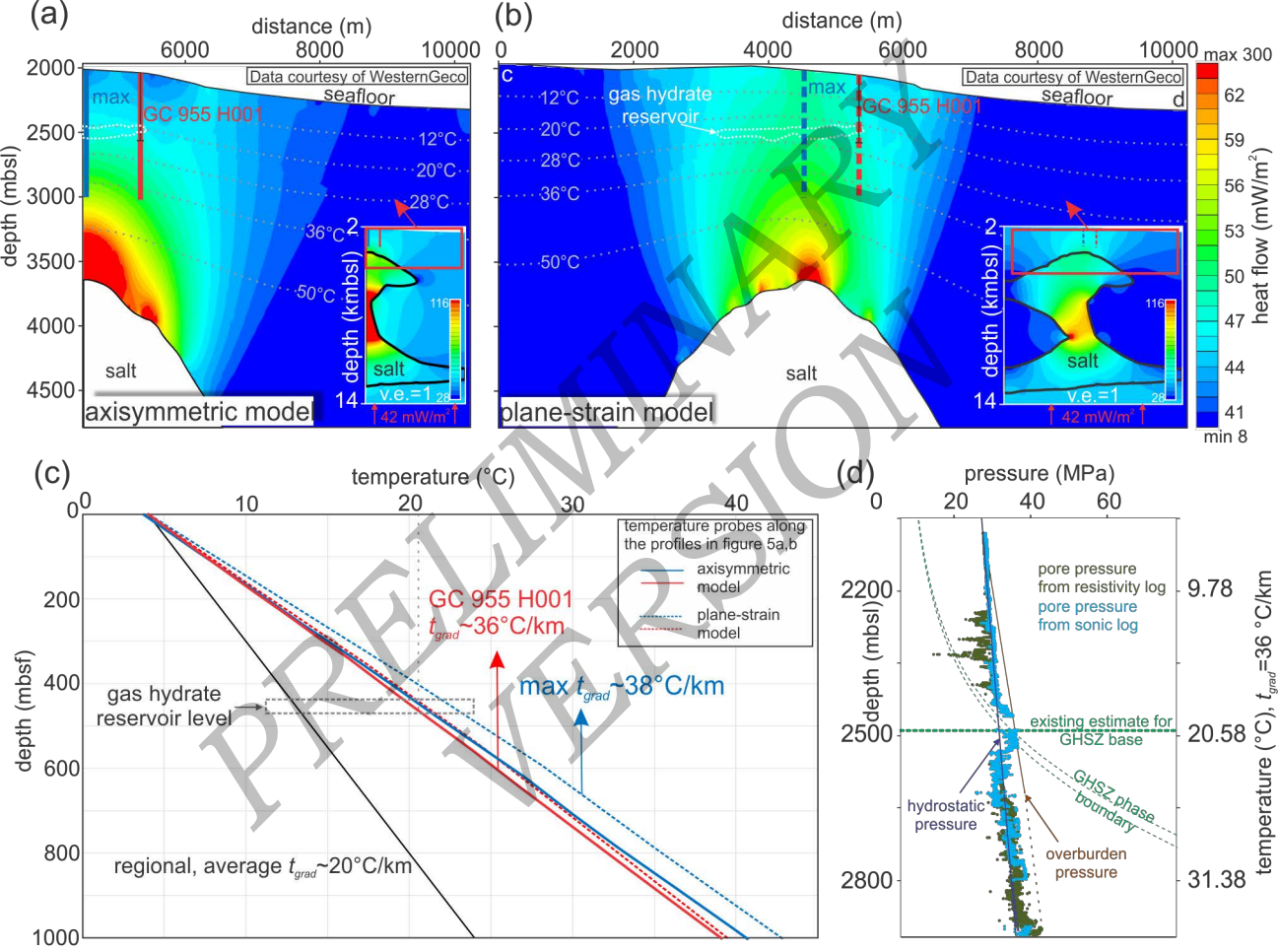

Figure 5

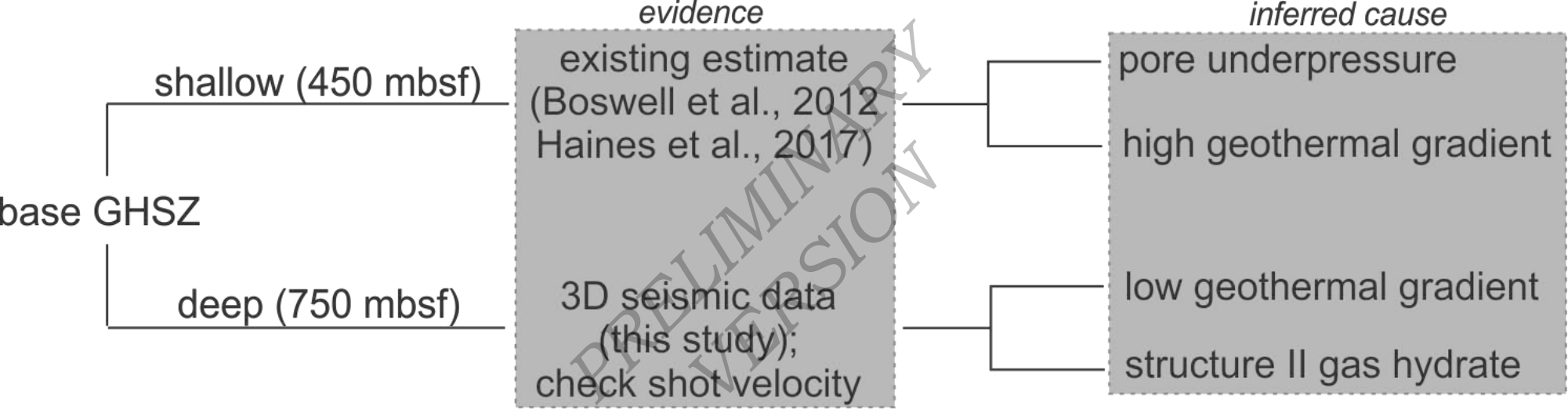
evidence
inferred cause
shallow (450 mbsf)
existing estimate
(Boswell et al., 2012
Haines et al., 2017)
pore underpressure
high geothermal gradient
base GHSZ
deep (750 mbsf)
3D seismic data
(this study);
check shot velocity
low geothermal gradient
structure II gas hydrate
PRELIMINARY
VERSION

Figure 6

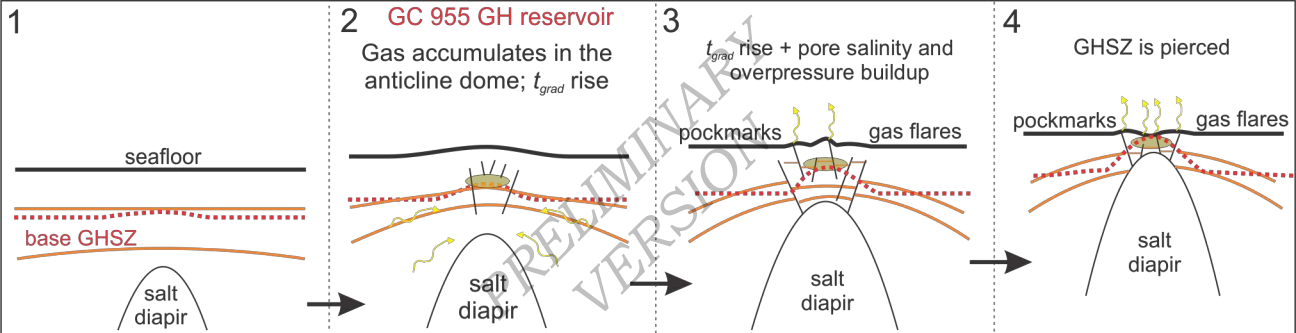
1
seafloor
base GHSZ
salt diapir
2
GC 955 GH reservoir
Gas accumulates in the anticline dome; t_{grad} rise
salt diapir
3
t_{grad} rise + pore salinity and overpressure buildup
pockmarks
gas flares
salt diapir
4
GHSZ is pierced
pockmarks
gas flares
salt diapir
PRELIMINARY VERSION

Figure 7

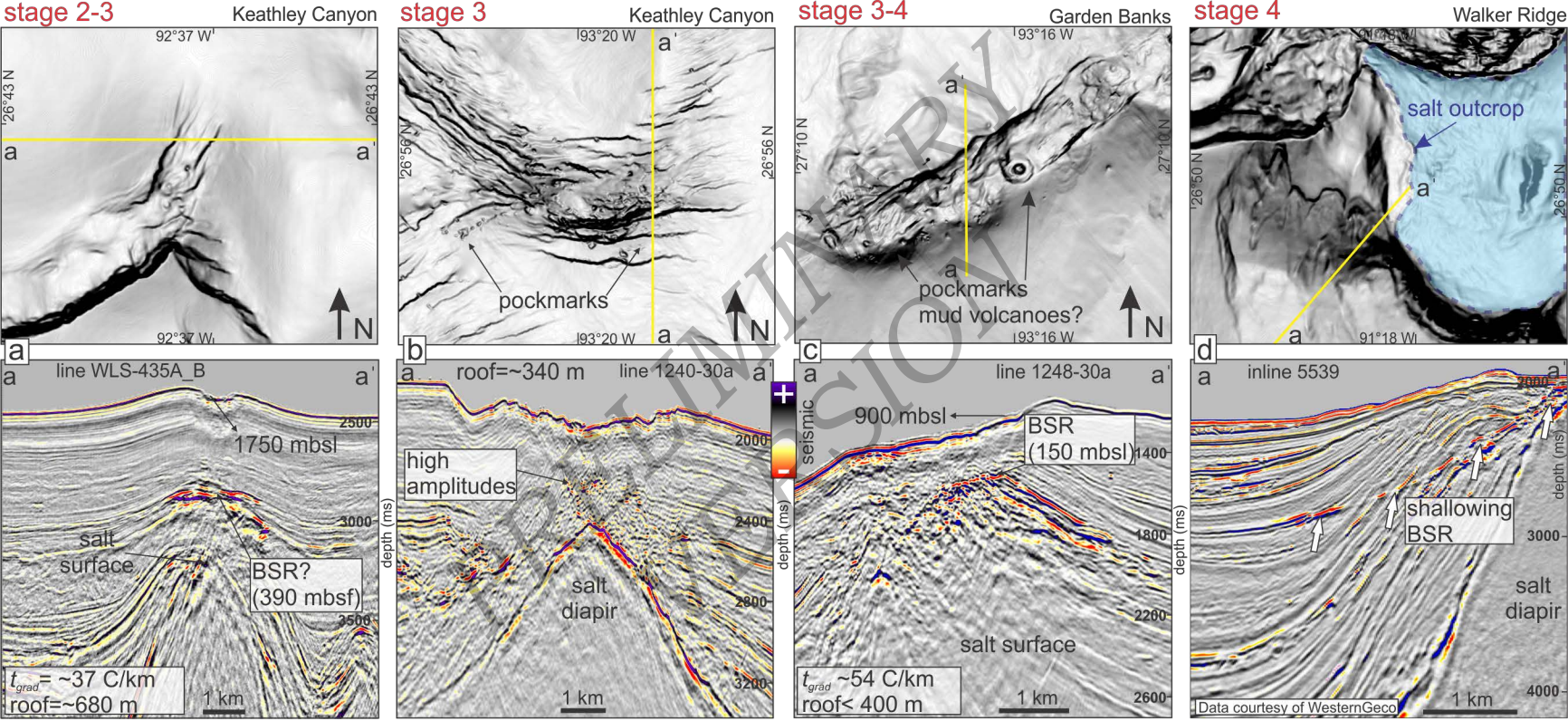

Figure 8